surface undergoes a compositional change and expansion indicate that exposed {00l} surfaces also participate in the dissolution process, at least initially.

This study has provided directly measured dissolution rates for surfaces on phlogopite, a silicate mineral, at room temperature. It has also shown that all phlogopite surfaces are reactive, including its basal surfaces. Each surface of phlogopite, or any other mineral, must behave according to the particular atomic structure, composition, and microtopography of that surface. Furthermore, the dissolution of each surface has a temporal dependence, although this effect may only be substantially variable in the early stages of dissolution. Finally, external factors must also come into play (for example, local conditions and proximal flow regimes), especially in natural settings (*21*). The concept and use of reactive surface area in silicate dissolution studies is now changing. It seems that, at least in the most favorable cases, the reactivity of various surface components can be cataloged and quantified. This opens the door to a new generation of rate equations and, ultimately, to a much better understanding of how minerals dissolve and influence our environment.

References and Notes

1. S. L. Brantley and Y. Chen, in *Chemical Weathering Rates of Silicate Minerals*, vol. 31 of *Reviews in Mineralogy*, A. F. White and S. L. Brantley, Eds. (Mineralogical Society of America, Washington, DC, 1995), chap. 4; A. F. White and M. L. Peterson, in *Chemical Modeling of Aqueous Systems II*, vol. 416 of *ACS Symposium Series*, D. C. Melchior and R. L. Bassett, Eds. (American Chemical Society, Washington, DC, 1990), chap. 35.
2. Some authors define reactive surface area as the area occupied by high-energy sites, such as defects and dislocation outcrops [W. H. Casey, M. J. Carr, R. A. Graham, *Geochim. Cosmochim. Acta* **52**, 1545 (1988)]. In surface complexation modeling, reactive sites consist of particular atomic arrangements where ligand adsorption and activated complex formation occur [C. M. Koretsky, D. A. Sverjensky, N. Sahai, *Am. J. Sci.* **298**, 349 (1998)]. Microscopic studies of the mineral-solution interface indicate that coordinatively unsaturated microtopographic configurations, such as kinks and steps, consist of the most reactive portion of a mineral surface [M. F. Hochella Jr., in *Mineral Surfaces*, vol. 5 of *Mineralogical Society Series*, D. J. Vaughan and R. A. D. Pattrick, Eds. (Chapman & Hall, New York, 1995), chap. 2]. In field-based studies, reactive surface area is the portion of the total mineral surface area that is in hydrologic contact with the system under study [J. I. Drever and D. W. Clow, in *Chemical Weathering Rates of Silicate Minerals*, vol. 31 of *Reviews in Mineralogy*, A. F. White and S. L. Brantley, Eds. (Mineralogical Society of America, Washington, DC, 1995), chap. 10].
3. G. Jordan and W. Ramansee, *Geochim. Cosmochim. Acta* **60**, 5055 (1996); Y. Liang, D. R. Baer, J. M. McCoy, J. E. Amonette, J. P. LaFemina, *ibid.*, p. 4883; A. Putnis, J. L. Junta-Rosso, M. F. Hochella Jr., *ibid.* **59**, 4623 (1995).
4. Real-time in situ dissolution of clay particles has been observed with AFM (D. Bosbach *et al.*, in preparation).
5. AFM images were collected with a NanoScope IIIa controller (Digital Instruments, Santa Barbara, CA) operating with TappingMode imaging and oxide-sharpened Si_3N_4 tips. Several images were collected in succession and compared to check for scanner drift and tip-induced erosion. XPS measurements were performed with a PHI 5400 x-ray photoelectron spectroscopy system (Perkin-Elmer, Eden Prairie, MN) using Al Kα radiation (1486.6 eV). Measurements were collected at 0°, 55°, and 75°, corresponding to approximate depths of analysis of 8.0, 4.5, and 2.0 nm, respectively [M. F. Hochella Jr. and A. H. Carim, *Surf. Sci.* **197**, L260 (1988)]. LEED spot patterns were collected with four-grid reverse-view LEED optics (OMICRON, Taunusstein, Germany) at beam energies between 50 and 150 eV.
6. M. Malmstrom and S. Banwort, *Geochim. Cosmochim. Acta* **61**, 2779 (1997).
7. B. E. Kalinowski and P. Schweda, *ibid.* **60**, 367 (1996).
8. J. G. Acker and O. P. Bricker, *ibid.* **56**, 3073 (1992).
9. See a review by K. L. Nagy, in *Chemical Weathering Rates of Silicate Minerals*, vol. 31 of *Reviews in Mineralogy*, A. F. White and S. L. Brantley, Eds. (Mineralogical Society of America, Washington, DC, 1995), chap. 5, and references therein.
10. In a comparative study of the reactivity of different surfaces on biotite, the edges were found to dissolve ~250 times as fast as the basal surfaces [M.-P. Turpault and L. Trotignon, *Geochim. Cosmochim. Acta* **58**, 2761 (1994)].
11. Etching was achieved by immersing the sample in 49% HF for 3 s, followed by a thorough rinsing with distilled-deionized H_2O. XPS analysis shows no increase in F content of the near surface, and all atomic ratios remain the same as those of unetched phlogopite, indicating that HF is not entering the structure. The LEED pattern is consistent with freshly cleaved phlogopite.
12. The solution [HCl (pH 2) or distilled water (pH 5.7) equilibrated with atmospheric CO_2] was introduced by means of a syringe and pumped at 10 ml $hour^{-1}$ with a low-flow peristaltic pump. Pumping was suspended during AFM image acquisition. When not imaging, the tip was withdrawn. Image quality degrades within 24 to 48 hours at pH 5.7, precluding long-term in situ experiments at this pH.
13. M. F. Hochella Jr., J. F. Rakovan, K. M. Rosso, B. R. Bickmore, E. Rufe, in *Mineral-Water Interfacial Reactions: Kinetics and Mechanisms*, vol. 715 of *ACS Symposium Series*, D. C. Sparks and T. J. Grundl, Eds. (American Chemical Society, Washington, DC, 1998), pp. 37–56.
14. This is achieved by using standard image analysis routines to measure the area, perimeter, and volume for each etch pit imaged. [J. C. Russ, *The Image Processing Handbook* (CRC Press, Ann Arbor, MI, ed. 3, 1995)].
15. Etch pit dimensions and dissolution rates are available at www.sciencemag.org/feature/data/1040546.shl.
16. A. Nonaka [*J. Colloid Interface Sci.* **99**, 335 (1984)] reports a roughness value (that is, ratio of BET surface area to geometric surface area) for mica of 1.08, so this estimate of BET-equivalent area should be reasonable.
17. A high flow rate coupled with a slow dissolution rate prevents saturation with respect to secondary phases at pH 2. Reaching saturation with respect to amorphous silica, for example, would require >100 layers of phlogopite to dissolve in static fluid filling the 0.03-ml fluid cell.
18. At 55°, Mg/Si decreases from 1.0 to 0.25, and Al/Si decreases from 0.33 to 0.21. K 2p and F 1s peaks are not discernable above the background. Si/O increases from 0.22 to 0.49.
19. W. H. Casey and B. Bunker, in *Mineral-Water Interface Geochemistry*, vol. 23 of *Reviews in Mineralogy*, M. F. Hochella Jr. and A. F. White, Eds. (Mineralogical Society of America, Washington, DC, 1990), chap. 10.
20. H. Kaviratna and T. J. Pinnavaia, *Clays Clay Miner.* **42**, 717 (1994).
21. M. F. Hochella Jr. and J. F. Banfield, in *Chemical Weathering Rates of Silicate Minerals*, vol. 31 of *Reviews in Mineralogy*, A. F. White and S. L. Brantley, Eds. (Mineralogical Society of America, Washington, DC, 1995), chap. 8.

22. We thank U. Becker, B. R. Bickmore, D. Bosbach, J. D. Rimstidt, J. L. Rosso, and K. M. Rosso for helpful discussions. We also thank B. R. Bickmore for developing some of the image analysis routines used in this study. The phlogopite sample was obtained from the Museum of Geological Sciences at Virginia Tech (sample HB-1246). Funding for this research was generously provided by the Petroleum Research Fund, administered by the American Chemical Society (grants PRF 31598-AC2 and 34326-AC2) and NSF (grants EAR-9527092 and EAR-9628023). This manuscript benefited from two anonymous reviewers.

1 April 1999; accepted 11 June 1999

Late Miocene Atmospheric CO_2 Concentrations and the Expansion of C_4 Grasses

Mark Pagani,*† Katherine H. Freeman, Michael A. Arthur

The global expansion of C_4 grasslands in the late Miocene has been attributed to a large-scale decrease in atmospheric carbon dioxide (CO_2) concentrations. This triggering mechanism is controversial, in part because of a lack of direct evidence for change in the partial pressure of CO_2 (pCO_2) and because other factors are also important determinants in controlling plant-type distributions. Alkenone-based pCO_2 estimates for the late Miocene indicate that pCO_2 increased from 14 to 9 million years ago and stabilized at preindustrial values by 9 million years ago. The estimates presented here provide no evidence for major changes in pCO_2 during the late Miocene. Thus, C_4 plant expansion was likely driven by additional factors, possibly a tectonically related episode of enhanced low-latitude aridity or changes in seasonal precipitation patterns on a global scale (or both).

Instability in Miocene climates is detailed by extensive stable isotope records (*1*) and is associated with turnovers in marine (*2*, *3*) and terrestrial biota (*4*), sea-level variability (*5*), and changes in surface- (*2*) and deep-water circulation (*6*). Short- and long-term climatic patterns are thought to reflect changes in CO_2 concentrations (*7–9*) or tectonically driven readjustments in ocean circulation (*6*, *10*). In particular, high-latitude climates gradually warmed during the early to middle Miocene [~24 to 15 million years ago (Ma)] and then

rapidly cooled as the East Antarctic ice sheet expanded during the middle Miocene (*11*).

Evidence suggests that C_4 grasses expanded rapidly during the late Miocene (~8 to 4 Ma) (*7*). Characterized by the Hatch-Slack photosynthetic pathway, C_4 plants (largely but not exclusively represented by grasses) can internally concentrate CO_2 before carbon is fixed by way of the Calvin cycle and subsequently avoid the energetic costs of photorespiration (*12*, *13*). This physiology provides C_4 plants with a competitive advantage over C_3 plants (which lack a CO_2-concentrating mechanism) when the ratio of atmospheric CO_2 to O_2 concentrations is low (*12*, *14*). Furthermore, the ability to increase internal leaf CO_2 concentrations allows C_4 plants to decrease their stomatal conductance, which effectively increases their water-use efficiency (*13*). Such adaptations provide an advantage under hot, high-irradiance, water-stressed conditions (*12*). The distribution of modern C_4 grasses on a global scale is most strongly correlated to minimum growing season temperatures, with high minimum temperatures favoring C_4 grasses (*15*).

The above physiological considerations led Cerling *et al.* (*7*) to attribute a global expansion of C_4 plants in the late Miocene to a decrease in the partial pressure of CO_2 (pCO_2) and to argue that crossing a critically low CO_2/O_2 threshold triggered an ecological response. Here we provide a record of alkenone-based pCO_2 estimates for the late Miocene (10 to 5 Ma) in combination with a pCO_2 record for the early to middle Miocene (*16*), and evaluate the role of pCO_2 as a mechanism forcing this ecological change.

The alkenone approach to estimating pCO_2 uses records of carbon isotopic fractionation during marine photosynthetic carbon fixation (ε_p). ε_p (expressed in per mil) for many marine algae is largely a function of the concentration of aqueous CO_2 in the growth medium ($[CO_{2aq}]$), cellular growth rate (*17*), and cell geometry (*18*). The isotopic composition of sedimentary organic carbon derived solely from specific photosynthetic marine organisms is best evaluated by isolating molecular biomarkers. When these biomarkers are unique to a particular group of organisms, one avoids the "noise" resulting from the integration of isotopic signals from an array of photosynthesizers with varying geometries, growth characteristics, and carbon fixation pathways. Long-chained unsaturated ketones (alkenones) represent one such class of biomarkers that are exclusively produced by some haptophyte algae in the modern ocean (*19*). ε_p records constructed from diunsaturated alkenones ($\varepsilon_{p37:2}$) have been used to determine variations in paleocean dynamics and Quaternary pCO_2 (*20*). Recent work, however, has provided an empirical expression of $\varepsilon_{p37:2}$ as a function of surface-water $[PO_4^{3-}]$ and $[CO_{2aq}]$ (*17*). Accordingly, reconstruction of paleo-pCO_2, which requires knowledge of past growth rates, can be constrained by estimating surface-water $[PO_4^{3-}]$. Our approach was to obtain $\varepsilon_{p37:2}$ from an oceanographic setting with long-term nutrient-limited conditions, such as those found in oligotrophic regions of mid-ocean gyres and inferred for our sample location. This approach minimizes the effect of growth rate on $\varepsilon_{p37:2}$, thereby leaving $[CO_{2aq}]$ as the primary control (*16*).

We studied samples from Deep Sea Drilling Project (DSDP) site 588 (26°06.7′S; 161°13.6′E; southwest Pacific). The low sedimentation rates (~2 cm/1000 years), character-

Department of Geosciences, The Pennsylvania State University, University Park, PA 16872, USA.

*Present address: Earth Science Department, University of California, Santa Cruz, CA 95064, USA.
†To whom correspondence should be addressed.

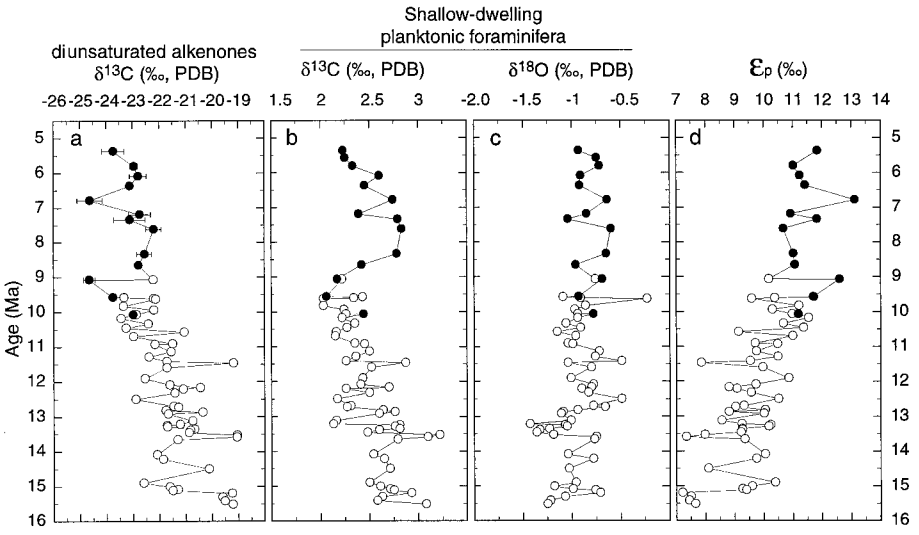

Fig. 1. (**A**) $\delta^{13}C$ values of heptatriaconta-15E, 22E-dien-2-ones (diunsaturated alkenones) from DSDP site 588 (*53*). PDB, pee dee belemnite. (**B**) $\delta^{13}C$ values of shallow-dwelling planktonic foraminifera from site 588. (**C**) $\delta^{18}O$ values for shallow-dwelling planktonic foraminifera. (**D**) ε_p record derived from diunsaturated alkenones (*53*). $\varepsilon_p = [(\delta d + 1000/\delta p + 1000) - 1] \times 10^3$, where δd is the carbon isotopic composition of CO_{2aq} calculated from planktonic foraminifera and δp is the carbon isotopic composition of haptophyte organic matter enriched by 4.2 per mil relative to alkenone $\delta^{13}C$ values (*54*). Points represent the average of values measured for each sample. ○, data from Pagani *et al.* (*16*); ●, results from this study.

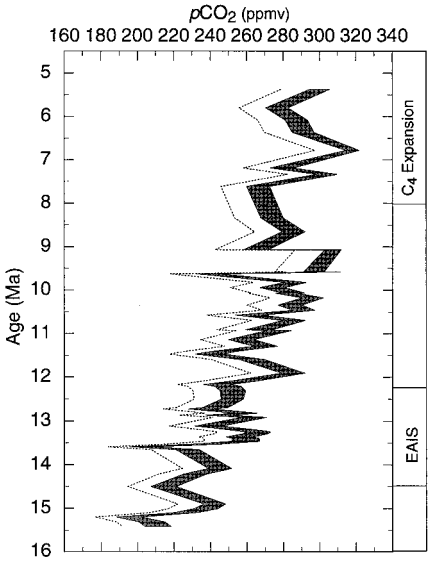

Fig. 2. Maximum pCO_2 estimates calculated on the basis of the ε_p record of site 588, where $\varepsilon_p = \varepsilon_f - b/[CO_{2aq}]$. The term b represents the sum of physiological factors, including growth rate (*17*) and cell geometry (*18*), that affect total carbon isotope discrimination. In the modern ocean, b is highly correlated to surface-water $[PO_4^{3-}]$ (*17*). pCO_2 values represented by the right edge of the shaded band are calculated with a value of 27 per mil for ε_f (the carbon isotope fractionation due to Rubisco), $[PO_4^{3-}] = 0.3$ μmol/l, and an equation for the physiological-dependent term b calculated with the upper 95% confidence limit from the global data set derived from all available data (*17*, *55*) ($b_{(27\ per\ mil)} = 4.35 \times [PO_4^{3-}]^2 + 125.65 \times [PO_4^{3-}] + 108.89$). Values on the left edge of the shaded band are calculated with a value of 25 per mil for ε_f, $[PO_4^{3-}] = 0.3$ μmol/l, and an equation for the physiological-dependent term b calculated with the upper 95% confidence limit from the global data set ($b_{(25\ per\ mil)} = 4.17 \times [PO_4^{3-}]^2 + 113.79 \times [PO_4^{3-}] + 88.63$). The dashed line represents pCO_2 estimates calculated with an equation for the physiological-dependent term b calculated with geometric mean regression of the global data set, a value of 25 per mil for ε_f, and a $[PO_4^{3-}] = 0.3$ μmol/l ($b_{(GM25\ per\ mil)} = 116.96 \times [PO_4^{3-}] + 81.42$). Values of CO_{2aq} were converted to pCO_2 by applying Henry's law with K_H (the temperature- and salinity-dependent CO_2 solubility coefficient) values (*56*) calculated assuming a salinity of 35 and surface-water temperatures derived from $\delta^{18}O$ values for planktonic foraminifera (Fig. 1C). Propagation of errors results in a 15% uncertainty for calculated pCO_2 values (*57*). EAIS, expansion of the East Antarctic ice sheet.

istic low organic-carbon contents (<0.1%) (*21*, *22*), and uniform deposition of nannofossil-foraminiferal oozes indicate deposition under oligotrophic water masses similar to conditions that characterize this site today. An age model was developed by linearly interpolating between magnetostratigraphic datums (*23*).

Our results (Figs. 1 and 2) show that pCO_2 steadily increased from a low at ~14 Ma [~180 parts per million by volume (ppmv)] and stabilized at concentrations between 320 and 250 ppmv during the late Miocene (9 Ma). These uniformly low pCO_2 values are consistent with middle to late Miocene alkenone-based pCO_2 estimates and trends from other localities (*16*), as well as late Miocene atmospheric CO_2 concentrations estimated from stomatal parameters of fossil oak leaves (*24*). In addition, other alkenone data suggest that pCO_2 decreased to about preindustrial levels near the end of the Oligocene (*16*). Therefore, assuming that models for C_4 versus C_3 plant competition are correct, low pCO_2 should have favored C_4 over C_3 floras by the early Miocene. However, because nearly 15 million years elapsed between the onset of low pCO_2 and the major C_4 plant expansion, it appears that pCO_2 level alone was not a sufficient trigger of the late Miocene event.

On the basis of phylogenetic data (*25*), fossil pollen evidence (*26*), and recent molecular isotopic data (*27*), the emergence of the C_4 photosynthetic pathway, as well as C_4 grasses, occurred before the Miocene. Accordingly, C_4 flora must have represented a component of vegetation in the early Neogene (*28*). For example, as much as a 10 to 30% C_4 dietary influence can be inferred from the carbon isotopic compositions of early to middle Miocene mammal tooth enamel (*29*). Nevertheless, carbon isotopic trends of paleosol carbonate (*30*–*32*), fossil mammal tooth enamel ($\delta^{13}C_{en}$) (*7*, *30*, *32*–*34*), and terrestrially derived organic matter (*35*) from Pakistan, South America, North America, and Africa support an interval of substantial ecological change to C_4-dominated vegetation (grasslands) between about 8 and 4 Ma. The character and pace of this change differed among localities (*32*), suggesting regional controls on the expansion of C_4 flora.

If the widespread expansion of C_4 plants was not a response to a sharp decrease in pCO_2, then we must seek another explanation for this change. In general, it is not necessarily justified to expect an immediate biological response (that is, diversification) after a physical forcing event (*36*). Therefore, it is possible that the timing of C_4 expansion was far removed from the conditions that promoted it. Alternatively, changes in climatic conditions, other than pCO_2, could have forced C_4 plant expansion. The most important modern environmental characteristics that favor C_4 plants include aridity for C_4 dicots and strong seasonal precipitation (that is, warm-season precipitation), with coinciding high minimum temperatures during the growing season for C_4 grasses (*12*, *37*). Changes in seasonal patterns of precipitation and temperature in key regions during the late Miocene can be inferred from a variety of data. For example, evolutionary trends in mammals (and other fauna) and floras from the middle to late Miocene suggest a pattern of increasing seasonality and aridity in North America, Europe, Africa, Pakistan, and Australia (*4*, *38*). Soil carbonate $\delta^{18}O$ data from Pakistan, Nepal, East Africa, Argentina, and the eastern Mediterranean (*31*, *32*, *39*), as well as tooth enamel $\delta^{18}O$ values from Argentina and North America (*32*), increase, suggesting increasing evaporation and aridity preceding and accompanying the expansion of C_4 flora. Dust fluxes, likely driven by the development of aridity in Asia and South America, increased in the North Pacific at 7.7 Ma (*40*) and peaked at about 8 Ma in the subtropical South Pacific (*41*). An increase in regional precipitation rates in North America (central Oregon and the Great Plains) is inferred from an increase in the depth of fossil soil calcic horizons at 7 to 6 Ma (*42*). We suggest that it was the development of low-latitude seasonal aridity and changes in growing conditions on a global scale, rather than a decrease in pCO_2, that led to the sudden expansion of C_4 vegetation at ~7 Ma.

Global climates could have been altered as a result of tectonic processes. For example, Ruddiman *et al.* (*43*), among others, have championed the role of late Cenozoic plateau uplift (southeast Asia and the American West) and other mountain-building events as major drivers of global climate change. Model simulations and paleoclimatic evidence imply that these uplifts altered zonal wind patterns, inducing strong seasonality in precipitation and aridity in many mid- to high-latitude regions in the Northern Hemisphere (*43*).

The timing of the major large-scale uplift events is controversial. Many studies have relied on the marine strontium isotope record, for example, as an indicator of greater uplift and weathering rates in the Himalaya-Tibetan Plateau (*9*). Trends in strontium isotope ratios indicate that substantial changes in the rate of ^{87}Sr increase occurred during two episodes in the Miocene (*44*) from about 21 to 17 Ma and 12 to 9 Ma. The first interval shows little indication of increased sediment yield to the ocean basins (*45*). The second, however, is associated with a number of indicators of uplift and increasing erosion rates on land (*40*, *41*), including a major increase in clastic sediment flux to the Indian Ocean basin (9 to 6 Ma) (*45*) [as well as a probable global increase (*46*)], an increase in Ge/Si ratios in opaline silica (8 to 4 Ma) (*47*), and a marked increase in pelagic phosphorous accumulation rates (8 to 4 Ma) (*48*). Therefore, we suggest that it was this late Miocene phase of Asian uplift, in conjunction with preexisting low pCO_2 levels, that caused the critical changes in climate patterns that favored C_4 plant expansion.

References and Notes

1. K. G. Miller, J. D. Wright, R. G. Fairbanks, *J. Geophys. Res.* **96**, 6829 (1991); J. D. Wright, K. G. Miller, R. G. Fairbanks, *Paleoceanography* **7**, 357 (1992).
2. R. Thunell and P. Belyea, *Micropaleontology* **28**, 381 (1982).
3. K. Wei and J. P. Kennett, *Paleoceanography* **1**, 67 (1986).
4. J. A. Wolfe, in *The Carbon Cycle and Atmospheric CO_2: Natural Variations Archean to Present*, E. T. Sundquist and W. S. Broecker, Eds. (American Geophysical Union, Washington, DC, 1985), pp. 357–373.
5. B. U. Haq, J. Hardenbol, P. R. Vail, *Science* **235**, 1156 (1987); K. G. Miller and P. J. Sugarman, *Geology* **23**, 747 (1995).
6. F. Woodruff and S. M. Savin, *Paleoceanography* **4**, 87 (1989).
7. T. E. Cerling *et al.*, *Nature* **389**, 153 (1997).
8. E. Vincent and W. H. Berger, in *The Carbon Cycle and Atmospheric CO_2: Natural Variations Archean to Present*, E. T. Sundquist and W. S. Broecker, Eds. (American Geophysical Union, Washington, DC, 1985), pp. 455–468.
9. M. E. Raymo, *Paleoceanography* **9**, 399 (1994).
10. J. D. Wright and K. G. Miller, *ibid.* **11**, 157 (1996).
11. N. J. Shackleton and J. P. Kennett, *Initial Rep. Deep Sea Drilling Proj.* **29**, 743 (1975).
12. M. D. Hatch, *Biochim. Biophys. Acta* **895**, 81 (1987).
13. C. C. Black, in *Regulation of CO_2 and O_2 by Photosynthetic Carbon Metabolism*, N. E. Tolbert and J. Preiss, Eds. (Oxford Univ. Press, Oxford, 1994), pp. 159–175.
14. R. W. Pearcy and J. Ehleringer, *Plant Cell Environ.* **7**, 1 (1984).
15. J. A. Teeri, in *Topics in Plant Population Biology*, O. T. Solbrig, S. Jain, A. B. Johnson, P. H. Raven, Eds. (Columbia Univ. Press, New York, 1979), pp. 357–374.
16. M. Pagani, M. A. Arthur, K. H. Freeman, *Paleoceanography* **14**, 273 (1999).
17. R. R. Bidigare *et al.*, *Global Biogeochem. Cycles* **11**, 279 (1997); R. R. Bidigare *et al.*, *ibid.* **13**, 251 (1999).
18. B. N. Popp *et al.*, *Geochim. Cosmochim. Acta* **62**, 69 (1998).
19. M. H. Conte, J. K. Volkman, G. Eglinton, in *The Haptophyte Algae*, J. C. Green and B. S. C. Leadbeater, Eds. (Clarendon, Oxford, 1994), pp. 351–377.
20. J. P. Jasper and J. M. Hayes, *Nature* **347**, 462 (1990); J. P. Jasper, A. C. Mix, F. G. Prahl, J. M. Hayes, *Paleoceanography* **6**, 781 (1994).
21. M. Pagani, thesis, Pennsylvania State University, State College (1998).
22. M. Pagani, K. H. Freeman, M. A. Arthur, *Geochim. Cosmochim. Acta*, in press.
23. C. E. Barton and J. Bloemendal, *Initial Rep. Deep Sea Drill. Proj.* **90**, 1273 (1986); S. C. Cande and D. V. Kent, *J. Geophys. Res.* **97**, 13917 (1992).
24. J. van der Burg, H. Visscher, D. L. Dilcher, W. M. Kürschner, *Science* **260**, 1788 (1993); W. M. Kürschner, J. van der Burgh, H. Visscher, D. L. Dilcher, *Mar. Micropaleontol.* **27**, 299 (1996).
25. E. A. Kellogg, in *C_4 Plant Biology*, R. F. Sage and R. K. Monson, Eds. (Academic Press, New York, 1999), pp. 411–444.
26. H. P. Linder, *Kew Bull.* **42**, 297 (1986); W. L. Crepet and G. D. Feldman, *Am. J. Bot.* **78**, 1010 (1991).
27. M. M. M. Kuypers, R. D. Pancost, J. S. Sinninghe Damastè, *Nature* **399**, 342 (1999).
28. J. D. Kingston, B. D. Marino, A. Hill, *Science* **264**, 955 (1994); M. E. Morgan, J. D. Kingston, B. D. Marino, *Nature* **367**, 162 (1994).
29. Organisms having a predominantly pure C_3 diet produce tooth enamel with a wide range of carbon isotope values ($\delta^{13}C_{en}$) (−15 to −8 per mil) ($\delta^{13}C = [(R_{sa}/R_{std}) - 1] \times 1{,}000$, where R represents the $^{13}C/^{12}C$ abundance ratio and subscripts sa and std represent the sample and pee dee belemnite stan-

dard, respectively). It has been argued that values greater than −8 per mil indicate the beginning of an unambiguous C_4 dietary signal (*7*). A $\delta^{13}C_{en}$ value of −8 per mil assumes a water-stressed, high light C_3 isotopic composition of ~−22 per mil (due, in part, to an assumed 1.5 per mil enrichment in ^{13}C of Miocene atmospheric CO_2 relative to today) and a fractionation of 14.3 per mil between plant and tooth enamel (*7*). However, the $\delta^{13}C$ values of terrestrial C_3 plants ($\delta^{13}C_{C3plant}$) range from ~−33 to −22 per mil, with the majority ranging between −28 and −26 per mil (*49*). Thus, a $\delta^{13}C_{C3plant}$ value of −22 per mil represents a highly conservative end member. Furthermore, available data support a range of values for the fractionation between mammalian diet and carbonate apatite ($\Delta_{plant\text{-}en}$ = 12 to 14.3 per mil) (*7*, *50*). Therefore, with the use of a less conservative approach, a tooth enamel $\delta^{13}C$ value of −8 per mil could constitute a 10 to 30% C_4 influence if one assumes an average $\delta^{13}C_{C3plant}$ = −25 per mil, a $\delta^{13}C_{C4plant}$ = −12 per mil, and maximum and minimum values for $\Delta_{plant\text{-}en}$ of 14 and 13 per mil, respectively.

30. T. E. Cerling, Y. Wang, J. Quade, *Nature* **361**, 344 (1993).
31. J. Quade, T. E. Cerling, J. R. Bowman, *ibid.* **342**, 163 (1989).
32. C. Latorre, J. Quade, W. C. McIntosh, *Earth Planet. Sci. Lett.* **146**, 83 (1997).
33. Y. Wang, T. E. Cerling, B. J. MacFadden, *Palaeogeogr. Palaeoclimatol. Palaeoecol.* **107**, 269 (1994).
34. B. J. MacFadden, Y. Wang, T. E. Cerling, F. Anaya, *ibid.*, p. 257.
35. C. France-Lanord and L. A. Derry, *Geochim. Cosmochim. Acta* **58**, 4809 (1994).
36. M. E. Patzkowsky, *Paleobiology* **21**, 440 (1995).
37. P. W. Hattersley, *Oecologia* **57**, 113 (1983); in *Desertified Grasslands: Their Biology and Management*, G. P. Chapman, Ed. (Academic Press, New York, 1992), pp. 181–212.
38. R. L. Bernor *et al.*, in *The Evolution of Western Eurasian Neogene Mammal Faunas*, R. L. Bernor, V. Fahlbusch, H.-W. Mittmann, Eds. (Columbia Univ. Press, New York, 1996), pp. 449–469; S. D. Webb, R. C. Hulbert, W. D. Lambert, in *Paleoclimate and Evolution*, E. S. Vrba, G. H. Denton, T. C. Partridge, L. H. Burckle, Eds. (Yale Univ. Press, New Haven, CT, 1995), pp. 91–108; D. I. Axelrod, *Bot. Rev.* **51**, 163 (1985); E. M. Van Zinderen and J. H. Mercer, *Palaeogeogr. Palaeoclimatol. Palaeoecol.* **56**, 217 (1986); L. J. Flynn and L. L. Jacobs, *ibid.* **38**, 129 (1982).
39. T. E. Cerling and J. Quade, *Chem. Geol.* **84**, 164 (1990); J. Quade, N. Soulounias, T. E. Cerling, *Palaeogeogr. Palaeoclimatol. Palaeoecol.* **108**, 41 (1994).
40. D. K. Rea, H. Snoeckx, L. H. Joseph, *Paleoceanography* **13**, 215 (1998).
41. D. K. Rea, *Rev. Geophys.* **32**, 159 (1994).
42. G. J. Retallack, *Palaios* **12**, 380 (1997).
43. W. F. Ruddiman, W. L. Prell, M. E. Raymo, *J. Geophys. Res.* **94**, 18409 (1989); W. F. Ruddiman, J. E. Kutzbach, I. C. Prentice, in *Tectonic Uplift and Climate Change*, W. F. Ruddiman, Ed. (Plenum Press, New York, 1997), pp. 204–235.
44. D. A. Hodell and F. Woodruff, *Paleoceanography* **9**, 405 (1994).
45. D. K. Rea, in *Synthesis of Results from Scientific Drilling in the Indian Ocean* (American Geophysical Union, Washington, DC, 1992), pp. 387–402.
46. T. A. Davies, W. W. Hayes, J. R. Southam, T. R. Worsley, *Science* **197**, 53 (1977).
47. A. Shemesh, R. A. Mortlock, P. N. Froelich, *Paleoceanography* **4**, 221 (1989).
48. G. M. Filippeli and M. L. Delaney, *ibid.* **9**, 643 (1994).
49. P. Deines, in *Handbook of Environmental Isotope Geochemistry,* P. Fritz and J. Fontes, Eds. (Elsevier, Amsterdam, 1980), pp. 329–345.
50. J. A. Lee-Thorp, J. C. Sealy, N. J. van der Merwe, *J. Archaeol. Sci.* **16**, 585 (1989); P. L. Koch, A. K. Behrensmeyer, M. L. Fogel, *Annu. Rep. Dir. Geophys. Lab. Carnegie Inst. Washington* **1990–1991**, 163 (1990–1991).
51. G. Mook, J. C. Bommerson, W. H. Staberman, *Earth Planet Sci. Lett.* **22**, 169 (1974); C. S. Romanek, E. L. Grossman, J. W. Morse, *Geochim. Cosmochim. Acta* **56**, 419 (1992).
52. J. Erez and B. Luz, *Geochim. Cosmochim. Acta* **47**, 1025 (1983).
53. Alkenones were recovered from sediments by Soxhlet extraction in a 2:1 aziotrope of methylene chloride and methanol. The total lipid extracts were separated by silica gel column chromatography into compound classes. Resulting ketone fractions were analyzed by gas chromatography. Shallow-dwelling planktonic foraminifera (*Globogerinoides quadrilobatus*) were selected from the 354- to 420-μm sieved fraction, and the resulting carbon isotopic compositions were used to calculate δd by assuming equilibrium conditions and applying temperature-dependent isotope equations (*51*). Mixed-layer temperatures were calculated from the $\delta^{18}O$ of *G. quadrilobatus* (*52*) assuming a value of 0 per mil [standard mean ocean water (SMOW)] for the oxygen isotope value of seawater. $\delta^{18}O = [R_{sa}/R_{std}) - 1] \times 1000$, where R represents the $^{18}O/^{16}O$ abundance ratio and subscripts sa and std represent the sample and SMOW standard, respectively.
54. B. N. Popp, F. Kenig, S. G. Wakeham, E. A. Laws, R. R. Bidigare, *Paleoceanography* **13**, 35 (1998).
55. B. N. Popp *et al.*, in *Reconstructing Ocean History: A Window into the Future*, F. Abrantes and A. Mix, Eds. (Plenum, New York, in press).
56. F. Weiss, *Mar. Chem.* **2**, 203 (1974).
57. Propagation of errors was determined with a Monte Carlo procedure. We assume uncertainties in our method, including the following: $[PO_4^{3-}]$, ±0.1; temperature (degrees Celsius), ±2; salinity, ±1; ε_f, ±1; analytical errors for $\delta_{37:2}$ and $\delta^{13}C_{foram}$ of ±0.5 per mil and ±0.2 per mil, respectively; and an 11% uncertainty about the slope and intercept of the b versus $[PO_4]$ geometric mean regression (representing the 95% confidence interval).
58. Samples for this project were provided by the DSDP/Ocean Drilling Program. This research was funded by grants from NSF and Joint Oceanographic Institutions/U.S. Science Advisory Committee. We would like to thank D. Walizer and G. Montemurro for their invaluable analytical assistance, L. Colorusso for helpful discussions, and P. Koch and J. Eigenbrode for their constructive comments and suggestions.

8 February 1999; accepted 17 June 1999

Hf Isotope Evidence for Pelagic Sediments in the Source of Hawaiian Basalts

J. Blichert-Toft,[1]* F. A. Frey,[2] F. Albarède[1]

Lead, oxygen, and osmium isotopic ratios measured on Hawaiian basalts can be matched with the isotopic ratios inferred for recycled ancient oceanic crust. High-precision hafnium isotopic data for lavas from several Hawaiian volcanoes identify old pelagic sediments in their source. These observations support the recycling hypothesis, whereby the mantle source of ocean island basalts includes ancient subducted oceanic crust. Hyperbolic lead-hafnium isotopic relations among Hawaiian basalts further indicate that upper mantle material is not involved in the production of hot spot basalts.

The apparently fixed position of hot spots on a global scale (*1*) and the constant drift velocity of their volcanoes (*2*) with respect to the underlying asthenosphere suggest that they originate deep in the mantle. The high $^3He/^4He$ ratios of ocean island basalts (OIBs) relative to those of mid-ocean ridge basalts (MORBs) (*3, 4*) reflect a relatively low $(U + Th)/^3He$ ratio in the OIB mantle, which may indicate that the lower mantle is less degassed than the upper mantle (*5*). This interpretation, which has provided a major constraint on models of mantle convection, conflicts with evidence that the source of OIBs is recycled oceanic lithosphere, material expected to be largely degassed. Trace element abundances (*6*) and isotopic ratios of Pb, Nd, and Hf (*7, 8*) indicate that primitive mantle is not the principal source of OIBs. Osmium isotopic measurements suggest that the source of OIBs is enriched in a component that was once extracted from the mantle as a liquid (*9*). Among the shields of Hawaiian volcanoes, the two extreme compositions are typified by the Mauna Kea and Koolau lavas, which fall at the opposite end-points of the Kea and Loa compositional trends, respectively (*10, 11*). The $^{187}Os/^{188}Os$ ratios and $\delta^{18}O$ of Koolau basalts are higher than in MORB, and these high values are characteristic of aged and altered oceanic crust (*9–11*). In contrast, the $\delta^{18}O$ of Mauna Kea basalts is lower than MORB values, possibly reflecting altered lower oceanic crust (*10*).

Oxygen and Os isotopes, however, cannot be used to distinguish between altered basaltic sections of the oceanic crust and the overlying deep-sea sediments (*11*), because it is the magnitudes of the isotopic shifts induced by these two components of the oceanic crust, and not their direction, that are the distinctive features. The recycling of sediments in the source of OIBs is an integral part of the initial formulation of the recycling hypothesis (*12, 13*). Sediments derived from continental detritus have distinctive Nb/U and Ce/Pb ratios compared with these ratios in basalts; however, these ratios in OIBs have been used to argue both for (*14*) and against (*15*) recycled continental ma-

[1]Ecole Normale Supérieure de Lyon, 69364 Lyon Cedex 7, France. [2]Massachusetts Institute of Technology, Cambridge, MA 02139, USA.

*To whom correspondence should be addressed. E-mail: jblicher@ens-lyon.fr